Atmos. Meas. Tech., 9, 3053–3062, 2016
www.atmos-meas-tech.net/9/3053/2016/
doi:10.5194/amt-9-3053-2016

Atmospheric Measurement Techniques
Open Access
EGU

Real time retrieval of volcanic cloud particles and SO_2 by satellite using an improved simplified approach

Sergio Pugnaghi[1], **Lorenzo Guerrieri**[1], **Stefano Corradini**[2], **and Luca Merucci**[2]

[1]Dipartimento di Scienze Chimiche e Geologiche, Università di Modena e Reggio Emilia, 41125 Modena, Italy
[2]Istituto Nazionale di Geofisica e Vulcanologia, 00143 Roma, Italy

Correspondence to: Sergio Pugnaghi (sergio.pugnaghi@unimore.it)

Received: 10 December 2015 – Published in Atmos. Meas. Tech. Discuss.: 17 February 2016
Revised: 6 June 2016 – Accepted: 20 June 2016 – Published: 15 July 2016

Abstract. Volcanic plume removal (VPR) is a procedure developed to retrieve the ash optical depth, effective radius and mass, and sulfur dioxide mass contained in a volcanic cloud from the thermal radiance at 8.7, 11, and 12 µm. It is based on an estimation of a virtual image representing what the sensor would have seen in a multispectral thermal image if the volcanic cloud were not present. Ash and sulfur dioxide were retrieved by the first version of the VPR using a very simple atmospheric model that ignored the layer above the volcanic cloud. This new version takes into account the layer of atmosphere above the cloud as well as thermal radiance scattering along the line of sight of the sensor. In addition to improved results, the new version also offers an easier and faster preliminary preparation and includes other types of volcanic particles (andesite, obsidian, pumice, ice crystals, and water droplets). As in the previous version, a set of parameters regarding the volcanic area, particle types, and sensor is required to run the procedure. However, in the new version, only the mean plume temperature is required as input data. In this work, a set of parameters to compute the volcanic cloud transmittance in the three quoted bands, for all the aforementioned particles, for both Mt. Etna (Italy) and Eyjafjallajökull (Iceland) volcanoes, and for the Terra and Aqua MODIS instruments is presented. Three types of tests are carried out to verify the results of the improved VPR. The first uses all the radiative transfer simulations performed to estimate the above mentioned parameters. The second one makes use of two synthetic images, one for Mt. Etna and one for Eyjafjallajökull volcanoes. The third one compares VPR and Look-Up Table (LUT) retrievals analyzing the true image of Eyjafjallajökull volcano acquired by MODIS aboard the Aqua satellite on 11 May 2010 at 14:05 GMT.

1 Introduction

The large volumes of ash and gases released into the atmosphere during explosive volcanic eruptions form clouds that can travel great distances from the source over long periods. These ash clouds can be generated at any time from the eruption of any one of more than 1200 active volcanoes scattered over the Earth's surface (Prata, 2009) and pose a real threat to air safety (Casadevall, 1994).

An effective global monitoring system today depends on the use of satellite data to detect and monitor the evolution of volcanic ash clouds. Timely information on the location, size, height, and ash content of potentially hazardous eruption clouds derived from satellite data are generated and used by the Volcanic Ash Advisory Centers to mitigate this type of threat and improve aviation safety (Francis et al., 2012).

Satellite sensors operating in the thermal infrared range are particularly effective for this purpose, when the interaction of volcanic ash with electromagnetic radiation makes it possible to detect and monitor volcanic clouds even at night. The algorithms developed exploit in various ways the reverse absorption of the brightness temperature observable in the channels centered at 11 and 12 microns. This feature is used both for discriminating ash and meteorological clouds (Prata 1989a, b) and for quantifying the mass, optical thickness, and effective radius of the ash contained in volcanic clouds (Wen and Rose, 1994; Yu et al., 2002).

Several algorithms were developed in the early efforts to detect volcanic clouds and retrieve the ash and SO_2 contents, as discussed in a recent critical review (Clarisse and Prata, 2016). Among the new algorithms, the simplified approach of the volcanic plume removal (VPR) is distinguished by its

ease of use and speed of calculation, making it highly effective for monitoring. Another advantage of the VPR approach is that it only requires the plume temperature as additional input, providing fresh estimates of ash and SO_2 as soon as new satellite images of an ongoing eruption become available (Pugnaghi et al., 2013; Guerrieri et al., 2015).

The VPR procedure was developed using thermal infrared (TIR) data collected by the Moderate Resolution Imaging Spectroradiometer (MODIS) instrument on board the Terra and Aqua polar platforms and by the Spinning Enhanced Visible and Infra-Red Imager radiometer (SEVIRI) on board meteorological satellites positioned on MSG geostationary orbits.

This paper aims to present the VPR procedure in an improved and simplified form as developed for the selected case studies of the Mt. Etna (Italy) and Eyjafjallajökull (Iceland) eruptions. Section 2 is dedicated to a theoretical description of the novel improvements of the VPR procedure, while Sect. 3 presents and discusses the results obtained for the validation case studies. In Sect. 4 the conclusions are provided. The VPR coefficients are tabulated in the Supplement for different types of plume particles (andesite, obsidian, pumice, ice, and water droplets), for both the Mt. Etna and Eyjafjallajökull volcanoes, and for the Terra and Aqua MODIS instruments.

2 Theory

The VPR procedure (Pugnaghi et al., 2013; Guerrieri et al., 2015) is a kind of linearization of the radiative transfer equation developed to retrieve, from multispectral satellite images at 8.7, 11, and 12 µm, the ash optical depth at 550 nm (δ^*), effective radius (R_e), mass (M_a), and sulfur dioxide mass (M_s) of a tropospheric volcanic cloud. The parameters required to apply the VPR are specific for a given area, type of plume particles, and sensor on board the satellite and these are easily determined a priori using the MODTRAN radiative transfer model. Once they have been computed, the only additional input required is the mean plume temperature.

Figure 1 shows the VPR procedure flowchart (dashed rectangle). Among the ancillary data, the land–sea mask is usually available with the radiance data while the operator has to define the plume mask and possibly the meteorological cloud mask. For the multispectral sensors the plume mask can be derived from ash detection techniques based on brightness temperature difference (see Prata, 1989b) and successive improvements (see Millington et al., 2012; Pavolonis et al., 2013), principle components analysis (Hillger and Clark 2002a, b), or neural networks (Picchiani et al., 2014). The volcanic cloud height can be obtained from visible/TIR ground-based cameras (Scollo et al., 2014), ground radar (Montopoli et al., 2014; Marzano et al., 2006; Corradini et al., 2016), lidar system (Scollo et al., 2012) measurements, or multispectral satellite data using different techniques like

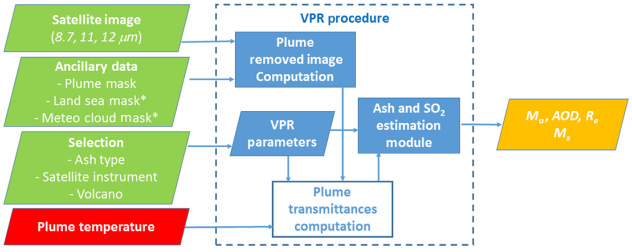

Figure 1. VPR I/O flowchart. Green: inputs given for a specific processing (the asterisk means optional input). Red: input to be computed. Orange: outputs.

"dark pixels" (Prata and Grant, 2001; Corradini et al., 2010), CO_2 slicing (Menzel et al., 1983; Platnick et al., 2003), H_2O intercept method (Nieman et al., 1993), tracking of volcanic cloud center of mass (Guerrieri et al., 2015), inversion schemes based on optimal estimation (Francis et al., 2012), or parallax-based methods with image pairs collected by LEO-GEO (Zakšek et al., 2013) and GEO-GEO (Merucci et al., 2016) instruments. Knowing the plume height, its temperature can be obtained from the available vertical atmospheric sounding.

The first steps of the VPR is the definition of the virtual image with the removed volcanic cloud and the computation of the plume transmittances for the three bands considered (8.7, 11, and 12 µm). In the earlier VPR approach, the atmosphere above the plume was assumed to be negligible and the results were adjusted with a cubic relationship, derived by fitting an adequate set of MODTRAN simulations (Pugnaghi et al., 2013; Guerrieri et al., 2015). The transmittance values at 11 and 12 µm were used to define maps of R_e, δ^*, and M_a, while the sulfur dioxide abundance map was estimated from the transmittance at 8.7 µm. Finally, the wind speed at the plume altitude was used to reconstruct the flux at the vents, considering both the ash mass and SO_2 maps (Merucci et al., 2013; Guerrieri et al., 2015; Merucci, 2015).

The novel VPR procedure described here applies a new atmospheric model for estimating volcanic cloud transmittance (white box, inside the dashed square in Fig. 1); the other steps are unchanged. In fact, the previous version assumed that τ, the transmittance of the whole atmosphere, was equal to τ', the transmittance of the atmospheric layer below the volcanic cloud. Here both the transmittance τ'' and the up-welling radiance L''_{uo} of the layer of atmosphere above the plume are considered (as shown in the scheme in Fig. 2). The term representing the surface thermal radiance scattered by the volcanic particles along the line of sight of the sensor is now also considered (not shown in the scheme of Fig. 2). This term is mainly proportional to $\varepsilon \cdot B(T_s) \cdot \tau$; ε is the surface emissivity, $B(T_s)$ is the Planck emission at the surface temperature T_s, and $\tau = \tau' \cdot \tau''$ is the transmittance of the whole atmosphere. The thermal radiance scattered towards the sensor strongly depends on the optical thickness of the volcanic

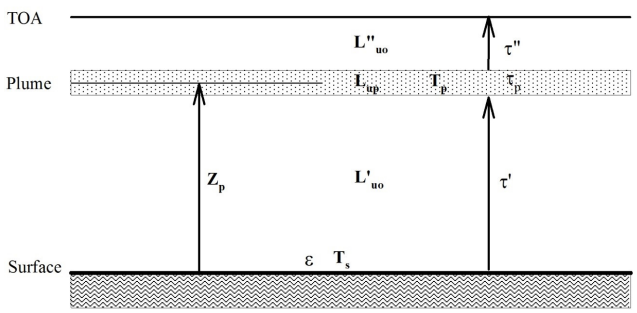

Figure 2. Scheme of the atmospheric model used in the improved VPR.

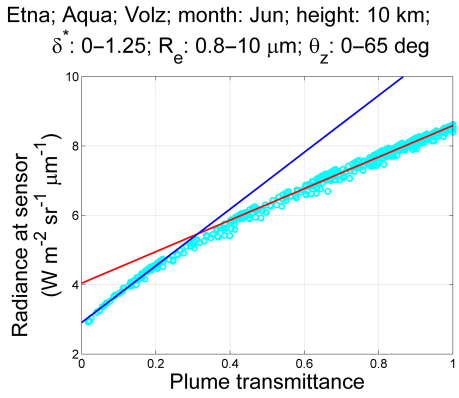

Figure 3. Radiances at the sensor (11 µm) vs. plume transmittances (cyan circles) with the two linear fits of Eq. (1) for the more transparent part of the plume (upper fit, red line) and Eq. (2) for the most opaque part of the plume (lower fit, blue line).

cloud; it is very important for optically thick (opaque) pixels. This term is absent when aerosol optical depth, δ, is 0.

In Fig. 2, $\tau_p = \tau_a \cdot \tau_s$ represents the total plume transmittance, where τ_a is the aerosol transmittance (liquid or solid particles contained in the volcanic cloud) and τ_s is the part due to sulfur dioxide. Clearly, when SO_2 is absent then $\tau_s = 1$, and when $\delta = 0$, then $\tau_a = 1$.

2.1 Absence of sulfur dioxide

Figure 3 shows a series of MODTRAN simulated radiances at the sensor vs. the plume transmittance obtained specifically for the band at 11 µm of the Aqua MODIS sensor, pumice (Volz, 1973) ash type, and a set of possible plume configurations (see Supplement for details).

The trend shown in Fig. 3 changes according to the state of the atmosphere, the surface characteristics and, of course, the vertical position of the volcanic cloud, composition, and ash content.

The radiance at the sensor (L_p), expresses as a function of the plume transmittance (τ_a), can be approximated with two linear trends. One for high radiance values (i.e., the transparent pixels of the plume) and one for low values (more opaque plume pixels). If the surface characteristics do not vary excessively over time, the linear trends always intersect close to the same transmittance value $\tau_t \approx 0.3$. Clearly, the gains and offsets of these two linear trends also change according to the state of the atmosphere, plume temperature, and so on. These two linear fits are characterized by four parameters. However, only the offset (named B_{up}) is required to fit the transparent part because the radiance L_0 is known from the plume removal part of the procedure. Similarly, when the intersection point of the two linear trends is known, the offset of the opaque part (named B_{dn}) is sufficient to determine the linear fit. As will be shown below, the two offsets B_{up} and B_{dn} can be computed knowing B_p, the Planck function, at T_p, the air temperature at the mean plume altitude.

In summary, by knowing the plume temperature T_p and the radiance L_o with the plume removed, it is possible to estimate the aerosol plume transmittance τ_a directly from the radiance L_p measured by the satellite without applying any atmospheric correction computed at runtime by radiative transfer models, but simply using Eq. (1) and, if necessary, Eq. (2) (respectively, red and blue lines of Fig. 3):

$$L_p = \left[L_o - B_{up}\right] \cdot \tau_a + B_{up}. \quad (1)$$

When the computed transmittance τ_a is lower than τ_t (intersection point), then the plume transmittance is recomputed by

$$L_p = \left[\left(L_t - B_{dn}\right)/\tau_t\right] \cdot \tau_a + B_{dn}, \quad (2)$$

where L_t is the radiance at the sensor computed using Eq. (1) for a plume transmittance $\tau_a = \tau_t$.

Figure 4a shows that in the 11 µm band there is a linear relationships between the two aforementioned offsets B_{up} and B_{dn}, and the Planck emission of the plume B_p, for the pumice and Mt. Etna volcano. A similar relationship also exists for the other two bands (obviously, for the band centered at 8.7 µm, sulfur dioxide must be absent) and for other volcanic particle types (see Supplement). Figure 4a shows that the plume transmittance at the intersection point τ_t has a small dependence on B_p too. Therefore

$$B_{up} = a_{up} \cdot B_p + b_{up}, \quad (3)$$

$$\tau_t = a_{tt} \cdot B_p + b_{tt}, \quad (4)$$

$$B_{dn} = a_{dn} \cdot B_p + b_{dn}. \quad (5)$$

The slope and offset values: a_{up}, b_{up}, a_{tt}, b_{tt}, a_{dn}, and b_{dn} of Eqs. (3), (4), and (5), for the three used MODIS bands and particle types and considered volcanoes are reported in Tables S1–S6 of the supplement. The last column of each table reports the correlation coefficients between the true transmittance of the volcanic clouds and the corresponding VPR retrievals.

2.2 Presence of sulfur dioxide

The presence of sulfur dioxide complicates transmittance retrieval at 8.7 µm because weak SO_2 absorption affects this

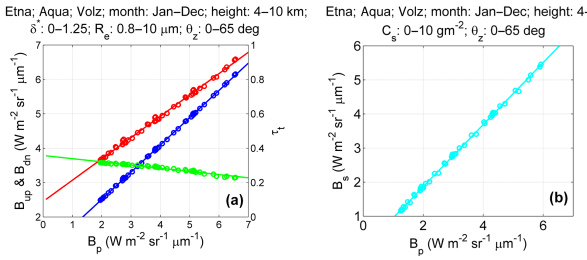

Figure 4. Linear trends of B_{up} (red), B_{dn} (blue), τ_t (green), and B_s (cyan) vs. B_p for 48 different plumes (12 months and 4 heights), each obtained from a set of MODTRAN simulations.

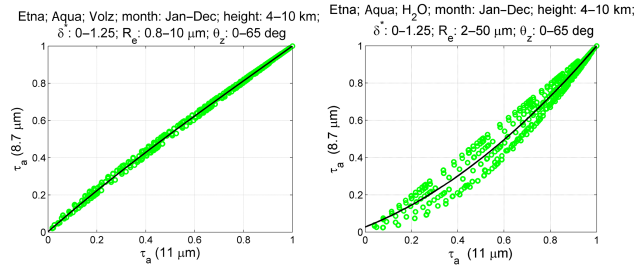

Figure 5. Scatter plots of the plume transmittance (obtained from a wide set of MODTRAN simulations) for Aqua MODIS bands at 11 and 8.7 µm for the pumice (Volz, 1973) ash type **(a)** and for water droplets **(b)**.

band. If the aerosol component of the plume transmittance at 8.7 µm is known, then the radiance at the sensor without the presence of sulfur dioxide (L_a) can be computed using the Eqs. (1) and (2). A knowledge of radiance due only to aerosols makes it possible to define the following simple equation:

$$L_p = [L_a - B_s] \cdot \tau_s + B_s, \quad (6)$$

where L_p is the total plume radiance measured by the sensor, L_a is radiance due to the aerosol components of the plume, and τ_s is the plume transmittance due to SO_2 absorption. B_s is a constant and represents the offset of the linear regression between the radiance at the sensor and the plume transmittance due to SO_2 absorption. Clearly B_s changes when the plume altitude, the state of the atmosphere above the plume, or the presence of the aerosol changes. To summarize, each plume has its own B_s and, also in this case, it is computed using a linear function of B_p:

$$B_s = a_s \cdot B_p + b_s. \quad (7)$$

The slope and offset values, a_s and b_s, for Mt. Etna and Eyjafjallajökull volcanoes are reported in Table S7 of the Supplement. Figure 4b shows the trend of B_s vs. B_p derived from a complete data set of MODTRAN simulations for Mt. Etna by considering the Aqua MODIS instrument.

Therefore, to compute τ_s from Eq. (6) it is necessary to know L_a which is derived from Eqs. (1) and (2) when τ_a for the band at 8.7 µm is known. The transmittance τ_a can easily be computed for pumice-type ash particles because a very good correlation exists between $\tau_{a,8.7}$ and $\tau_{a,11}$ (see Fig. 5a, and Pugnaghi et al., 2013).

Unfortunately, for the other particle types considered (see Supplement), the correlation between $\tau_{a,8.7}$ and $\tau_{a,11}$ is not always good, as in the example of Fig. 5b showing the scatter plot for water droplets. Nevertheless, it should be noted that this correlation becomes very good when only particles of the same effective radius R_e are considered.

In these cases with non-pumice ash types, the aerosol transmittance $\tau_{a,8.7}$ at 8.7 µm can be obtained from the following formula:

$$\tau_{a,8.7} = e^{-\mu \cdot \delta_{8.7}} = e^{-\mu \cdot m_{8.7} \cdot \delta^*}, \quad (8)$$

where μ is the optical air mass factor, $\delta_{8.7}$ is the vertical optical depth, δ^* is the vertical optical depth at 550 nm, and $m_{8.7}$ is the gain of the linear relationship which gives the optical depth $\delta_{8.7}$, when δ^* is known; the gain $m_{8.7}$ is a function of the effective radius R_e and is known from the MODTRAN simulations (Guerrieri et al., 2015).

To sum up, the novel VPR procedure first computes the 11 and 12 µm band transmittances and from these the aerosol optical depth at 550 nm (δ^*) and the effective radius (R_e) of each pixel of the plume (Pugnaghi et al., 2013); then the aerosol transmittance at 8.7 µm ($\tau_{a,8.7}$) is obtained using Eq. (8). Finally, the transmittance $\tau_{s,8.7}$ (derived from Eq. 6) is used to estimate the SO_2 columnar abundance C_s, given the proper absorption coefficient β (Pugnaghi et al., 2013) and the optical air mass μ factor.

$$\tau_{s,8.7} = e^{-\mu \cdot \beta \cdot C_s} \quad (9)$$

The subsequent steps of the VPR procedure have not been changed and can be found in Pugnaghi et al. (2013). Nevertheless, to conclude the theoretical discussion, it is important to note the superposition effect of ash and sulfur dioxide on the radiance measured by the sensor. This means that the proposed VPR procedure can also work well in cases of a "double-plume" at different temperatures, for example when an ash plume is located directly above or below a sulfur dioxide plume.

3 Validation test procedures

Three test procedures were defined to validate the improved version of the VPR. The first one is, as described in Pugnaghi et al. (2013), a comparison between the ash and SO_2 parameters set to perform the MODTRAN simulations and the corresponding values obtained from the new VPR retrievals (Sect. 3.1). The second test is based on the comparison between the retrievals obtained from the old and new version of the VPR procedure by considering two-trial synthetic images, as described in Corradini et al. (2014), depicting a uniform ocean surface under a cloudless sky, with a real

Table 1. Five central bins of the distributions of the differences (VPR retrievals minus true values) for the optical depth and the effective radius, obtained from the simulations performed for the Sicilian Mt. Etna volcano cases.

	Ash				Solid and liquid water	
δ^*	Pumice (%)	Andesite (%)	Obsidian (%)	δ^*	Ice (%)	H_2O (%)
−0.4	2.5	1.4	2.6	−0.4	0	0
−0.2	10.1	5.0	7.4	−0.2	0	0
0.0	81.0	87.6	84.2	0.0	93.4	92.2
0.2	1.8	3.1	1.8	0.2	3.5	6.5
0.4	1.5	0	0.7	0.4	1.1	1.3
R_e (µm)	Pumice (%)	Andesite (%)	Obsidian (%)	R_e (µm)	Ice (%)	H_2O (%)
−2	0.6	0.3	0	−6	1.4	0
−1	6.2	2.7	7.8	−3	5.6	1.2
0	70.8	83.4	68.4	0	68.7	88.7
1	18.5	4.9	22.4	3	13.4	0.3
2	1.3	1.4	0.9	6	4.0	0.1

atmosphere characteristic for Mt. Etna and Eyjafjallajökull volcano areas (Sect. 3.2). Finally, a comparison between the retrievals realized using the new VPR and the consolidated LUT approach, applied to a real image collected during the 2010 Eyjafjallajökull eruption, is realized (Sect. 3.3).

3.1 Validation procedure using simulated radiances

The coefficients a and b reported in Tables S1–S7, respectively the gain and offset of Eqs. (3), (4), (5), and (7), are calculated using a wide set of MODTRAN simulations. This set represents the mean climatological characteristics of the area around the considered volcano, a 1 km depth volcanic cloud located at different heights, and the volcanic cloud seen by the satellite sensor under different viewing angles. For each particle type, simulations were carried out considering 9 effective radius R_e, 8 optical depths δ^* (aerosol optical depth at 550 nm), and 10 values of SO_2 columnar contents C_s (see Supplement for a detailed description).

Each MODTRAN simulation contains the total transmittance of the atmospheric path ($\tau \cdot \tau_p = (\tau' \cdot \tau'') \cdot (\tau_a \cdot \tau_s)$, see Fig. 2) and the up-welling (L_u) and down-welling (L_d) radiances. Assuming as known the surface temperature T_s and the emissivity ε, the radiance L_p measured by the sensor is obtained from the radiative transfer Eq. (10):

$$L_p = [\varepsilon \cdot B(T_s) + (1-\varepsilon) \cdot L_d] \cdot \tau \cdot \tau_p + L_u. \quad (10)$$

To calculate the radiance L_p, the climatological monthly mean temperature of the ocean surface close to the considered volcano (Mt. Etna or Eyjafjallajökull) has been used, with an ocean surface emissivity set to 0.98.

From L_p, the new VPR version is used to retrieve effective radius R_e, the optical depth δ^*, and the SO_2 columnar content C_s. The distributions of the differences between the VPR retrievals and the input data (R_e, δ^*, C_s) show a good performance of the procedure.

Table 1 shows that for Mt. Etna volcano and for all the tested ash types and solid and liquid water particles, the percentage of cases is well described by the five central bins of the computed distributions. The central bin of the distribution represents the zero difference between retrievals and true input values. The width of the distribution bins is ±0.1 for the optical depth and ±0.5 and ±1.5 µm for ash and ice crystals/water droplets effective radii, respectively. Table 2 shows the same distributions but for the Eyjafjallajökull volcano. In Table 2 an extra column named "Eyja" shows the results for a kind of ash collected in the Eyjafjallajökull area after the 2010 eruption (D. Peters, private communication, 2013); it must be underlined that "Eyja" ash and andesite have quite similar optical characteristics.

Table 3 shows the main three central channels of the distributions of the differences between the VPR SO_2 columnar abundances and the true values. When no particles are present in the volcanic cloud or when the ash transmittance is perfectly known, the agreement (difference lower than ±0.5 g m^{-2}) is very high: 96 and 97 % for Mt. Etna and Eyjafjallajökull, respectively. Therefore, considering pure SO_2 clouds, Eqs. (6), (7), and (9) fit the simulations very well. This good result reduces to about 50 % when the SO_2 is mixed to ice crystals in a volcanic cloud of Mt. Etna. In the presence of SO_2 mixed with pumice (Mt. Etna) or "Eyja" ash (Eyjafjallajökull) the percentage reduces to about 60–70 %. The worst result shown is due to the approximations performed to calculate the ash or ice transmittance $\tau_{a,8.7}$ at 8.7 µm.

3.2 Validation procedure using synthetic images

The second test procedure uses two synthetic images, and, as in the previous test, the main aspect is the knowledge of the particle type contained in the volcanic cloud and its optical characteristics. However, in this case the values of R_e, δ^*,

Table 2. Five central bins of the distributions of the differences (VPR retrievals minus true values) for the optical depth and the effective radius, obtained from the simulations performed for the Icelandic Eyjafjallajökull volcano cases. "Eyja" represents a kind of ash collected in the Eyjafjallajökull area after the 2010 eruption (D. Peters, private communication, 2013).

	Ash					Solid and liquid water	
δ^*	Pumice (%)	Andesite (%)	Obsidian (%)	Eyja (%)	δ^*	Ice (%)	H_2O (%)
−0.4	2.7	1.3	2.5	1.3	−0.4	0	0
−0.2	12.5	7.3	9.3	8.2	−0.2	1.2	0
0.0	78.1	84.9	82.1	82.5	0.0	92.4	91.9
0.2	2.9	4.0	2.5	4.5	0.2	3.2	7.0
0.4	0.8	2.1	0.7	2.2	0.4	1.1	1.0
R_e (µm)	Pumice (%)	Andesite (%)	Obsidian (%)	Eyja (%)	R_e (µm)	Ice (%)	H_2O (%)
−2	0.9	0	0.1	0	−6	1.5	0.1
−1	6.2	2.1	7.3	0.3	−3	5.3	1.8
0	71.6	85.8	71.0	85.1	0	67.7	88.4
1	18.4	4.2	20.5	7.7	3	14.4	0.1
2	0.8	1.3	0.8	2.4	6	3.8	0.1

Table 3. Three central bins of the distributions of the differences (VPR retrievals minus true values) for the SO_2 columnar abundance, obtained from the simulations performed for the Sicilian Mt. Etna and the Icelandic Eyjafjallajökull volcanoes.

	Mt. Etna			Eyjafjallajökull	
SO_2 (g m^{-2})	SO_2 only (%)	SO_2 and pumice (%)	SO_2 and ice (%)	SO_2 only (%)	SO_2 and Eyja (%)
−1	3.0	21.5	18.0	2.1	15.8
0	96.4	59.0	50.0	97.4	72.6
1	0.6	7.4	12.2	0.4	5.4

and C_s do not correspond exactly to the input data used in the MODTRAN simulations but instead are randomly chosen.

A real atmosphere, an ocean temperature, and an ash type typical of the Mt. Etna volcano characterize the first synthetic image, while the second is adapted to match the Eyjafjallajökull volcano. Since the volcanic clouds can often contain water droplets or crystal of ice, this test has been doubled, assuming a similar plume for the Mt. Etna volcano composed first of ash and SO_2 (ash/SO_2) and then of ice and SO_2 (ice/SO_2). Currently VPR does not permit us to compute two different types of aerosol in the same pixel.

In the synthetic image of Mt. Etna, the plume was defined as 1 km thick, located between 7 and 8 km and containing pumice ash (Volz, 1973) and SO_2. The columnar abundance of sulfur dioxide ranges from 1 to 10 g m^{-2} while the ash optical depth δ^* varies from 0.1 to 1.5; therefore, a minimal quantity of sulfur dioxide and ash is always present in the plume. The effective radii R_e of the spherical ash particles have a uniform distribution, on a logarithmic scale, in the range 0.8–7 µm. A similar volcanic cloud is used for the plume composed of SO_2 and ice. The only difference is the dimension of the ice crystals, which have an effective radius ranging from about 1.4 to 50 µm. The atmosphere used to build this synthetic image is the one measured on 26 October 2013 at 12:00 GMT at the WMO station of Trapani (western tip of Sicily). The plume shape and geometry is the real shape and geometry of the Mt. Etna eruption cloud recorded by the MODIS aboard the Aqua satellite at 12:20 GMT of the same day.

Table 4 compares the retrieval of the new and old VPR procedures for both ash/SO_2 and ice/SO_2 test cases. As this table shows, all the ash, ice, and SO_2 parameters retrieved using the new VPR are closer to the true values, except for the total SO_2 mass retrieved from the ash/SO_2 synthetic image. In this case, the greater error on ash mass leads to an erroneous compensation on the SO_2 mass that accidentally becomes closer to the true value.

The second synthetic image is for the Eyjafjallajökull volcano. In this case the plume was again defined as 1 km thick but located between 4 and 5 km and composed of andesite (Pollack et al., 1973) and SO_2. For this volcanic cloud, the same ranges and distributions of SO_2 columnar content, ash optical depth δ^*, and effective radius R_e were used as for Mt. Etna, and the results are reported in Table 5. The ice and SO_2 plume results are not shown in this case because the parameters required by the old version of the VPR were not available. The atmosphere used to build this synthetic image is the one measured on 11 May 2010 at 12:00 GMT at the WMO

Table 4. Main characteristics of synthetic image, indicated as "true", together with the results of the VPR procedure, both new and old versions. The percentage differences are shown in brackets.

	Pumice test case			Ice test case		
	True	VPR new	VPR old	True	VPR new	VPR old
Mean R_e (μm) (% difference)	2.85	2.92 (2.5)	4.80 (68.4)	10.39	12.61 (21.4)	14.60 (40.5)
Mean δ^* (% difference)	0.25	0.22 (−12)	0.19 (−24)	0.25	0.25 (0)	0.22 (−12)
Ash mass (t) (% difference)	8336	7812 (−6.3)	7166 (−14.0)	11 394	12 237 (7.4)	13 945 (22.4)
Pixels detected with ash/ice	7533	7533	7317	7533	7533	7317
SO_2 mass (t) (% difference)	19 636	17 146 (−12.7)	18 880 (−3.9)	19 636	16 780 (−14.5)	15 010 (−23.6)
Pixels detected with SO_2	7533	7533	7533	7533	7436	7533

Mt. Etna on 23 October 2013; plume altitude 7–8 km

Table 5. Main characteristics of synthetic image, indicated as "true", together with the results of the VPR procedure, both new and old versions. The percentage differences are shown in brackets.

	True	VPR new	VPR old
Mean R_e (μm) (% difference)	2.83	2.62 (−7.4)	3.3 (16.6)
Mean δ^* (% difference)	0.28	0.29 (+3.6)	0.39 (39.3)
Ash mass (t) (% difference)	13 227	12 006 (−9.2)	9674 (−26.9)
Pixels detected with ash	10 624	10 624	6532
SO_2 mass (t) (% difference)	30 724	28 714 (−6.5)	28 235 (−8.1)
Pixels detected with SO_2	10 624	10 624	9827

Eyjafjallajökull: andesite; 11 May 2010, 14:05; plume altitude 4–5 km

station of Keflavik (Iceland). The plume shape and geometry is the real shape and geometry of the Eyjafjallajökull eruption cloud recorded by the MODIS aboard the Aqua satellite at 14:05 GMT of the same day.

As Table 5 shows, the new VPR version generates better estimations of all the parameters compared to the old VPR approach.

3.3 Validation procedure using a real case

During April–May 2010 the Eyjafjallajökull volcanic cloud plume induced the cancellation of more than 100 000 flights over Europe, about half of the total air traffic (Carboni et al., 2012).

The 2010 Eyjafjallajökull (63°38′ N; 19°36′ W) eruption started around mid-April and lasted about 40 days. In the 2 weeks from 5 to 20 May the most important eruptive phase occurred. In this period the eruptive column, with heights in the 4–10 km range (Stohl et al., 2011), was characterized by a copious production of ash. The Aqua MODIS image collected on 11 May 2010 at 14:05 UTC has been analyzed using both VPR and LUT (Corradini et al., 2009, 2010) procedures. The two approaches assumed the presence of andesite (Pollack et al. 1973) ash in the volcanic cloud and used the same mean cloud altitude of 5 km. The main difference is that the atmospheric correction, needed to run the LUT procedure, is obtained from the local atmospheric vertical profiles (pressure, temperature, and relative humidity) measured from the closest WMO station (Keflavik) to the satellite acquisition (in space and time), while the VPR procedure uses only the air temperature at the mean plume altitude at runtime.

Table 6. Retrievals obtained by LUT and VPR procedures.

	LUT	VPR
Mean R_e (μm)	3.0	2.8
Mean δ^*	1.0	1.2
Ash mass (t)	50 481	51 910
SO_2 mass (t)	56 116	62 518

Eyjafjallajökull: andesite; 11 May 2010, 14:05; plume altitude 4.5–5.5 km.

Figure 6 shows the maps of δ^* (a), R_e (b), M_a (c), and M_s (d) retrieved with the VPR procedure. The maps obtained from LUT procedure show the same structure, and Table 6 reports the retrievals of both procedures. The total ash and SO_2 masses differ of about the 3 and 10 %, respectively.

Figure 7 shows the ash and SO_2 fluxes at the craters calculated with the two procedures. All the fluxes have been calculated assuming a constant velocity of 20.6 ($m\,s^{-1}$), which is the wind speed measured at Keflavik at the plume height of 5 km. As figure shows, both the ash and SO_2 trends show a good correlation.

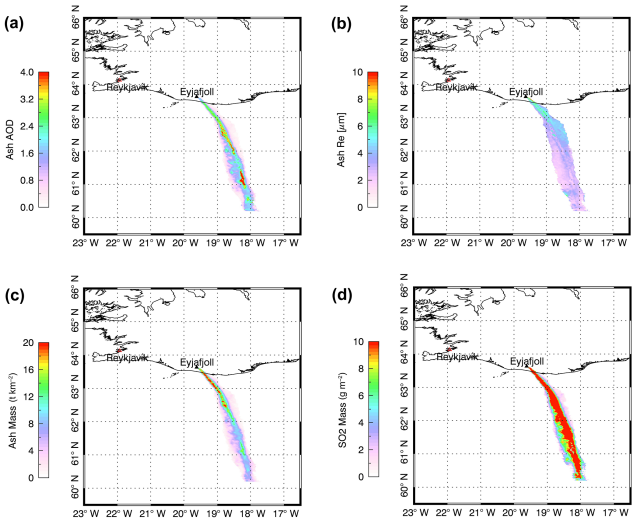

Figure 6. Maps of ash aerosol optical depth at 550 nm **(a)**, effective radius **(b)**, mass **(c)**, and sulfur dioxide mass **(d)** calculated with the VPR procedure. From Aqua MODIS over Eyjafjallajökull on 11 May 2010 at 14:05 GMT.

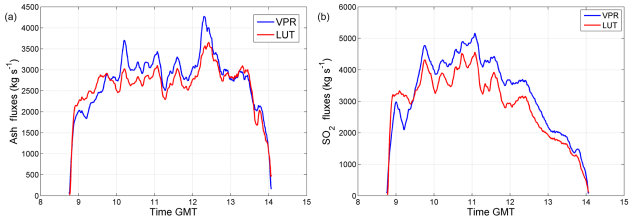

Figure 7. Ash **(a)** and SO_2 **(b)** fluxes at the craters calculated with the two procedures, LUT and VPR (Merucci et al., 2011).

Carboni et al. (2012) proposed a new scheme for sulfur dioxide retrieval from IASI measurements applied to Eyjafjallajökull volcano 2010 eruption. By applying this method to the portion of IASI image equivalent to the portion of MODIS image in Fig. 6, the estimated sulfur dioxide is 8768 tons (E. Carboni, private communication, May 2016), a value which is very different from the retrievals of Table 6. Andesite is the most widely ash type used in the Icelandic volcanoes (Thomas et al., 2011; Francis et al., 2012; Millington et al., 2012), and the optical characteristics of the ash collected by D. Peters (private communication, 2013) in the area of the Eyjafjallajökull volcano after the 2010 eruption are similar to those of andesite proposed by Pollack et al. (1973). However, different types of material were observed during the different days of the Eyjafjallajökull eruption (Borisova et al., 2012). Often the mass of ash in a volcanic cloud does not change so much as the ash type; vice versa, the mass of SO_2 is strongly affected by the optical characteristics of the considered ash. A simple example can clarify the situation. Assuming the volcanic cloud of Fig. 6 to be containing pumice (Volz, 1973) instead of andesite (Pollack et al., 1973), the estimated total mass of sulfur dioxide reduces to 9824 tons, which is very close to the value retrieved by Carboni et al. (2012).

4 Conclusions

The new VPR version presented here is an approximated procedure that easily allows us to estimate the main characteristics of volcanic particle clouds, including andesite, pumice, obsidian, and Eyja ash types, ice and water droplets, and volcanic SO_2 clouds. It uses only the mean altitude cloud temperature as input to directly interpret MODIS TIR multispectral images and retrieves particle effective radius, optical depth, mass of the volcanic cloud particle utilized, and mass of sulfur dioxide contained in each pixel. The VPR approach requires no atmospheric correction because this is implicit in the procedure itself. The retrieval of effective radius, optical depth, and sulfur dioxide abundance is derived from the estimation of the plume transmittances in the bands centered at 8.7, 11, and 12 μm. In this paper a novel and effective improvement in the transmittance estimation scheme is presented. The plume transmittance is obtained from the radiance measured by the sensor using two simple linear relationships, which represent the thickest and the most transparent part of the plume, respectively. These two linear trends account for two minor terms which were not considered in the previous version: the layer of atmosphere above the plume and the thermal radiance scattered along the line of sight of the sensor. The approximation for very thick/opaque volcanic clouds (transmittances lower than 0.05) is less effective. The improvement involves the computation of volcanic cloud transmittance, while no other parts of the previous procedure have been modified. In particular, the proposed improvement has two positive and relevant effects: (1) it is easier to use and provides more accurate results than before; (2) the preliminary work to compute the parameters required by the procedure (the parameters reported in Supplement) is even easier and requires less computation time.

The new VPR procedure was validated by considering simulated radiances, synthetic images, and real data.

The distributions of the differences between the VPR retrievals and the input data (R_e, δ^*, C_s) used for the simulated radiances computation show good performances of the new VPR. The correlation coefficient between the transmittance of the volcanic cloud simulated by MODTRAN radiative transfer code and the corresponding transmittance retrieved by the VPR procedure in nearly all cases is close to one, as reported in the last columns of Tables S1–S7.

The percentage difference between the average input data of the synthetic images and the mean results of the novel VPR ranges between 0 and 21 %, while the old VPR ranges between 4 and 68 % (see Tables 4 and 5), confirming the improved performance of the new version.

Finally, the novel VPR was compared to the established LUT procedure in the real case of the 2010 Eyjafjallajökull eruption by analyzing the results obtained with the Aqua MODIS image collected on 11 May 2010 at 14:05 UTC, assuming an andesite-ash-type cloud and the same mean cloud altitude of 5 km. The ash aerosol optical depth, effective radius, maps, and the SO_2 mass maps retrieved with VPR and LUT procedures show that the same structure and the total ash and SO_2 masses differ by about the 3 and 10 %, respectively. Moreover, the ash and SO_2 fluxes at the craters have been calculated and are in good agreement.

The Supplement related to this article is available online at doi:10.5194/amt-9-3053-2016-supplement.

Acknowledgements. This work was partially funded by the European Union's Seventh Framework Programme (FP7/2007-2013) through the project APhoRISM (Advanced PRocedures for volcanIc and Seismic Monitoring) under grant agreement number 606738.

Edited by: A. Kokhanovsky
Reviewed by: three anonymous referees

References

Borisova, A. Y., Toutain, J.-P., Stefansson, A., Gouy, S., and de Parseval, P.: Processes controlling the 2010 Eyjafjallajökull explosive eruption, J. Geophys. Res., 117, B05202, doi:10.1029/2012JB009213, 2012

Carboni, E., Grainger, R., Walker, J., Dudhia, A., and Siddans, R.: A new scheme for sulphur dioxide retrieval from IASI measurements: application to the Eyjafjallajökull eruption of April and May 2010, Atmos. Chem. Phys., 12, 11417–11434, doi:10.5194/acp-12-11417-2012, 2012.

Casadevall, T. J.: The 1989–1990 eruption of Redoubt Volcano, Alaska: impacts on aircraft operations, J. Volcanol. Geotherm. Res., 62, 301–316, 1994.

Clarisse, L. and Prata, A. J.: Infrared sounding of volcanic ash, in: Volcanic Ash: Hazard Observation, edited by: Mackie S., Cashman K., Ricketts H., Rust A., and Watson M., Elsevier, 27 May, 2016.

Corradini, S., Merucci, L., and Prata, A. J.: Retrieval of SO_2 from thermal infrared satellite measurements: correction procedures for the effects of volcanic ash, Atmos. Meas. Tech., 2, 177–191, doi:10.5194/amt-2-177-2009, 2009.

Corradini, S., Merucci, L., Prata, A. J., and Piscini, A.: Volcanic ash and SO_2 in the 2008 Kasatochi eruption: retrievals comparison from different IR satellite sensors, J. Geophys. Res., 115, D00L21, doi:10.1029/2009JD013634, 2010.

Corradini, S., Pugnaghi, S., Piscini, A., Guerrieri, L., Merucci, L., Picchiani, M., and Chini M.: Volcanic Ash and SO_2 retrievals using synthetic MODIS TIR data: comparison between inversion procedures and sensitivity analysis, Ann. Geophys., 57, doi:10.4401/ag-6616, 2014.

Corradini, S., Montopoli, M., Guerrieri, L., Ricci, M., Scollo, S., Merucci, L., Marzano, F. S., Pugnaghi, S., Prestifilippo, M., Ventress, L. J., Grainger, R. G., Carboni, E., Vulpiani, G., and Coltelli, M.: A Multi-Sensor Approach for Volcanic Ash Cloud Retrieval and Eruption Characterization: The 23 November 2013 Etna Lava Fountain, Remote Sens., 8, 58, doi:10.3390/rs8010058, 2016.

Francis, P. N., Cooke, M. C., and Saunders, R. W.: Retrieval of physical properties of volcanic ash using Meteosat: A case study from the 2010 Eyjafjallajökull eruption, J. Geophys. Res., 117, D00U09, doi:10.1029/2011JD016788, 2012.

Guerrieri, L., Merucci, L., Corradini, S., and Pugnaghi, S.: Evolution of the 2011 Mt. Etna ash and SO_2 lava fountain episodes using SEVIRI data and VPR retrieval approach, J. Volcanol. Geoth. Res., 291, 63–71, doi:10.1016/j.jvolgeores.2014.12.016, 2015.

Hillger, D. W. and Clark, J. D.: Principal component image analysis of MODIS for volcanic ash – Part I: Most important bands and implications for future GOES Imagers, J. Appl. Meteorol., 41, 985–1001, doi:10.1175/1520-0450(2002)041<0985:PCIAOM>2.0.CO;2, 2002a.

Hillger, D. W. and Clark, J. D.: Principal component image analysis of MODIS for volcanic ash – Part II: Simulation of current GOES and GOES-M imagers, J. Appl. Meteorol., 41, 1003–1010, doi:10.1175/1520-0450(2002)041<1003:PCIAOM>2.0.CO;2 , 2002b.

Marzano, F. S., Barbieri, S., Vulpiani, G., and Rose, W. I.: Volcanic ash cloud retrieval by ground-based microwave weather radar, IEEE T. Geosci. Remote, 44, 3235–3246, doi:10.1109/TGRS.2006.879116, 2006.

Menzel, W. P., Smith, W. L., and Stewart, T. R.: Improved cloud motion wind vector and altitude assignment using VAS, J. Appl. Meteorol., 22, 377–384, 1983.

Merucci, L.: Volcanic risk mitigation and insights into volcanic processes from space-based measurements, PhD. Thesis, Università degli Studi di Modena e Reggio Emilia, ESS XXVII ciclo, 2015.

Merucci, L., Burton, M., Corradini, S., and Salerno, G. G.: Reconstruction of SO_2 flux emission chronology from space-based measurements, J. Volcanol. Geoth. Res., 206, 80–87, doi:10.1016/j.jvolgeores.2011.07.002, 2011.

Merucci, L., Zakšek, K., Carboni, E., and Corradini, S.: Stereoscopic Estimation of Volcanic Ash Cloud-Top Height from Two Geostationary Satellites, Remote Sens., 8, 206, doi:10.3390/rs8030206, 2016.

Millington, S. C., Saunders, P. N. F. R. W., and Webster H. N.: Simulated volcanic ash imagery: A method to compare NAME ash concentration forecasts with SEVIRI imagery for the Eyjafjallajokull eruption in 2010, J. Geophys. Res., 117, D00U17, doi:10.1029/2011JD016770, 2012.

Montopoli, M., Vulpiani, G., Cimini, D., Picciotti, E., and Marzano, F. S.: Interpretation of observed microwave signatures from ground dual polarization radar and space multi-frequency radiometer for the 2011 Grímsvötn volcanic eruption, Atmos. Meas. Tech., 7, 537–552, doi:10.5194/amt-7-537-2014, 2014.

Nieman, S. J., Schmetz, J., and Menzel, W. P.: A comparison of several techniques to assign heights to cloud tracers, J. Appl. Meteor., 32, 1559–1568, 1993.

Pavolonis, M., Heidinger, A., and Siegla, J.: Automated retrievals of volcanic ash and dust cloud properties from upwelling infrared measurements, J. Geophys. Res., 118, 1436–1458, doi:10.1002/jgrd.50173, 2013.

Picchiani, M., Chini, M., Corradini, S., Merucci, L., Piscini, A., and Del Frate, F.: Neural network multispectral satellite images classification of volcanic ash plumes in a cloudy scenario, Ann. Geophys., 57, doi:10.4401/ag-6638, 2014.

Platnick, S., King, M. D., Ackerman, S. A., Menzel, W. P., Baum, B. A., Riédi, J. C., and Frey, R. A.: The MODIS Cloud Products: Algorithms and Examples from Terra, IEEE T. Geosci. Remote, 41, 459–473, 2003.

Pollack, J., Toon, O., and Khare, B.: Optical properties of some terrestrial rocks and glasses, Icarus, 19, 372–389, doi:10.1016/0019-1035(73)90115-2, 1973.

Prata, A. J.: Observations of volcanic ash clouds in the 10–12 µm window using AVHRR/2 data, Int. J. Remote Sens., 10, 751–761, 1989a.

Prata, A. J.: Infrared Radiative Transfer Calculations for Volcanic Ash Clouds, Geophys. Res. Lett., 16, 1293–1296, 1989b.

Prata, A. J.: Satellite detection of hazardous volcanic clouds and the risk to global air traffic, Nat. Hazards, 51, 303–324, 2009.

Prata, A. J. and Grant, I. F.: Determination of mass loadings and plume heights of volcanic ash clouds from satellite data, CSIRO Atmospheric Research Technical Papers No. 48, CSIRO Marine and Atmospheric Research, 2001.

Pugnaghi, S., Guerrieri, L., Corradini, S., Merucci, L., and Arvani, B.: A new simplified approach for simultaneous retrieval of SO_2 and ash content of tropospheric volcanic clouds: an application to the Mt Etna volcano, Atmos. Meas. Tech., 6, 1315–1327, doi:10.5194/amt-6-1315-2013, 2013.

Scollo, S., Boselli A., Coltelli M., Leto, G., Pisani, G., Spinelli, N., and Wang, X.: Monitoring Etna volcanic plumes using a scanning LiDAR, Bull. Volcanol., 74, 2383–2395, doi:10.1007/s00445-012-0669-y, 2012.

Scollo, S., Prestifilippo, M., Pecora, E., Corradini, S., Merucci, L., Spata, G., and Coltelli, M.: Eruption Column Height Estimation: the 2011-2013 Etna lava fountains, Ann. Geophys., 57, S0214, doi:10.4401/ag-6396, 2014.

Stohl, A., Prata, A. J., Eckhardt, S., Clarisse, L., Durant, A., Henne, S., Kristiansen, N. I., Minikin, A., Schumann, U., Seibert, P., Stebel, K., Thomas, H. E., Thorsteinsson, T., Tørseth, K., and Weinzierl, B.: Determination of time- and height-resolved volcanic ash emissions and their use for quantitative ash dispersion modeling: the 2010 Eyjafjallajökull eruption, Atmos. Chem. Phys., 11, 4333–4351, doi:10.5194/acp-11-4333-2011, 2011.

Thomas, H. E. and Prata, A. J.: Sulphur dioxide as a volcanic ash proxy during the April–May 2010 eruption of Eyjafjallajökull Volcano, Iceland, Atmos. Chem. Phys., 11, 6871–6880, doi:10.5194/acp-11-6871-2011, 2011.

Volz, F. E.: Infrared optical constants of ammonium sulfate, Sahara dust, volcanic pumice and fly ash, Appl. Opt., 12, 564–568, 1973.

Wen, S. and Rose, W. I.: Retrieval of sizes and total masses of particles in volcanic clouds using AVHRR bands 4 and 5, J. Geophys. Res., 99, 5421–5431, 1994.

Yu, T., Rose, W. I., and Prata, A. J.: Atmospheric correction for satellite-based volcanic ash mapping and retrievals using "split window" IR data from GOES and AVHRR, J. Geophys. Res., 107, 4311, doi:10.1029/2001JD000706, 2002.

Zakšek, K., Hort, M., Zaletelj, J., and Langmann, B.: Monitoring volcanic ash cloud top height through simultaneous retrieval of optical data from polar orbiting and geostationary satellites, Atmos. Chem. Phys., 13, 2589–2606, doi:10.5194/acp-13-2589-2013, 2013.